HYPERPARALLEL TEMPERING MONTE CARLO AND ITS APPLICATIONS

Qiliang Yan and Juan J. de Pablo

Department of Chemical Engineering, University of Wisconsin–Madison, Madison, Wisconsin 53706

This review discusses a newly proposed class of tempering Monte Carlo methods and their application to the study of complex fluids. The methods are based on a combination of the expanded grand canonical ensemble formalism (or simple tempering) and the multidimensional parallel tempering technique. We first introduce the method in the framework of a general ensemble. We then discuss a few implementations for specific systems, including primitive models of electrolytes, vapor–liquid and liquid–liquid phase behavior for homopolymers, copolymers, and blends of flexible and semiflexible polymers. © 2001 Academic Press.

I. Introduction

Complex fluids such as electrolyte solutions, polymer solutions, and biological macromolecule solutions pose significant obstacles to molecular

ADVANCES IN CHEMICAL ENGINEERING, VOL. 28 0065-2377/01 $35.00

simulation, particularly at low temperatures and elevated densities. Conventional molecular dynamics methods are unable to generate trajectories that are long enough to cover the inherently long characteristic relaxation times that characterize polymeric fluids, and naïve Monte Carlo techniques are unable to sample their configuration space efficiently. All of these systems, however, are of engineering importance. Unfortunately, these are also systems for which our theoretical understanding is far from complete. Predictive models for the equilibrium thermodynamic and structural properties of such fluids are required to design chemical and separation processes; to formulate new models, it would be useful to have access to the results of simulations.

When only the equilibrium properties of a complex fluid are of interest, it is possible to devise "nonphysical" simulation techniques that are sometimes able to circumvent the sampling problems that are usually associated with complex fluids. Examples of such techniques include configurational bias Monte Carlo methods, multicanonical ensemble simulations, J-walking, $1/k$ sampling, simulated tempering, and parallel tempering [1–14]. In this review we discuss some of our recent experiences with parallel tempering. This method has a number of useful features, which make it attractive for the study of complex fluids. Interestingly, while the idea of parallel tempering is not new [8, 9], its application to the study of many-body fluids has been limited. We therefore present results for a variety of systems, and in each case we try to emphasize the advantages provided by tempering over more conventional techniques.

The basic idea of parallel tempering consists of simulating several copies of a system in parallel; each copy or "replica" is constructed to represent the same system in a different thermodynamic state. Conventional Monte Carlo methods are employed to sample the configuration of each distinct replica under the relevant thermodynamic conditions. In addition to the trial moves involved in such methods, however, attempts are made to interchange the configurations corresponding to any two replicas of the system. Such trial "swaps" are accepted according to probability criteria that ensure the appropriate ensembles are sampled. The benefit of swapping is that if one of the replicas relaxes much faster than the others (e.g., a replica at a high temperature), the fast-evolving configurations in that replica can be artificially "propagated" to other boxes via exchanges, thereby effectively accelerating the relaxation of all other copies of the system.

Depending on the system and the ensemble of choice, the thermodynamic state of a replica can be specified through the number of molecules of each species, the volume, the temperature, the pressure, and the chemical potential. Our experience (and that of others [15, 16]) suggests that, from the point of view of improving sampling, open ensembles offer a number

of advantages over closed systems. In open ensembles, molecules can be completely removed from a system and reinserted at a later point in completely different positions and configurations, thereby circumventing diffusional bottlenecks. Furthermore, for difficult systems, such as polymers, deletions, and insertions can be facilitated significantly by resorting to expanded ensemble methods [17, 18]. Most of the implementations of hyperparallel tempering Monte Carlo (HPTMC) reported here are carried out in open ensembles, and whenever possible we also capitalize on the benefits provided by configurational bias and expanded ensemble techniques. As discussed in this review, it turns out that in some cases HPTMC can provide striking efficiency increases over traditional methods for the simulation of complex fluids with minimal changes to existing simulation algorithms and codes.

II. Methodology

Formally, we consider a generalized ensemble whose partition function is given by

$$Z(\mathbf{f}) = \sum_x \Omega(x) w(x, \mathbf{f}), \tag{1}$$

where $\mathbf{f}$ denotes a set of specified generalized forces or potentials, which determine the thermodynamic state of the system. In Eq. (1), x is used to denote a microscopic state or an instantaneous configuration of the system, $\Omega(x)$ is the density of states, and $w(x, \mathbf{f})$ is an arbitrary weighting function for state x, at the given set of generalized potentials $\mathbf{f}$. The grand canonical ensemble is recovered by writing

$$\mathbf{f} = \{T, \mu\}, \qquad w(x, \mathbf{f}) = \exp(-\beta U(x) + N(x)\beta\mu), \tag{2}$$

where $\beta = 1/k_B T$, T is the temperature, k_B is Boltzmann's constant, μ is the specified chemical potential, $U(x)$ is the potential energy corresponding to configuration x, and $N(x)$ is the number of particles in configuration x.

Hyperparallel tempering simulations are conducted on a composite ensemble, which consists of M, noninteracting replicas of the above-mentioned generalized ensemble. Each replica can have a different set of generalized potentials. The complete state of the composite ensemble is specified through $\mathbf{x} = (x_1, x_2, ..., x_M)^T$, where x_i denotes the state of the ith replica. The partition function Z_c of the composite ensemble is given by

$$Z_c = (\mathbf{f}_1, \mathbf{f}_2, \cdots, \mathbf{f}_M) = \prod_{i=1}^{M} Z(\mathbf{f}_i). \tag{3}$$

The unnormalized probability density of the complete state **x** is proportional to

$$p(\mathbf{x}) \prod_{i=1}^{M} \Omega(x_i) w(x_i, \mathbf{f}_i). \tag{4}$$

In expanded grand canonical ensemble simulations [18] (also called simple tempering simulations), the system can jump along a set of expanded states, in addition to the conventional (N, U) phase-space variables of a grand canonical ensemble. For the particular implementation to polymeric fluids, chain molecules are inserted or removed gradually, i.e., several segments at a time. In other words, a simulation box contains several "regular" chain molecules and a tagged chain, whose length n_y fluctuates during the simulation; n_y therefore serves as the expanded state variable. A preweighting factor $\exp(\Psi(y))$ is assigned to each expanded state y. In the language of Eq. (1), the weighting function for the expanded grand canonical ensemble is

$$\mathbf{f} = \{T, \mu, \Psi\}, \qquad w(x, \mathbf{f}) = \exp[-\beta U(x) + N(x)\beta\mu + \Psi(y)]. \tag{5}$$

If we assume that the segmental chemical potential is independent of chain length, we can set the preweighting function to be

$$\Psi(y) = \frac{n_y}{n}\beta\mu^r = \frac{n_y}{n}\left[\beta\mu - \ln\left(\frac{N_y}{V}\right)\right], \tag{6}$$

where $N_y = N + n_y/n$; n_y is the length of the tagged chain and n is the length of a full polymer chain. In Eq. (6), μ^r denotes the residual chemical potential of a polymer chain.

Figure 1 illustrates schematically the implementation of HPTMC. Each box in the figure represents a replica of the simulation system; each replica has a different value of T, μ, and n_y. To implement a hyperparallel tempering algorithm, three types of trial moves are necessary. (1) Conventional canonical Monte Carlo moves are used to sample configurations in each replica of the system. These moves include translational or rotational displacements and configurational-bias or reptation moves for polymers. (2) Trial shrinking or growing moves are proposed to change the length of a tagged chain in each replica, thereby implementing the underlying expanded grand canonical formalism. (3) Configuration swaps or exchanges are attempted between any two randomly chosen replicas. The arrows in Fig. 1 correspond to different types of moves.

The acceptance criteria corresponding to trials moves of type 1 or 2 are fairly standard and have been reported in a number of texts and articles. We therefore limit the remainder of this section to a brief discussion of the acceptance criteria for trial swap moves. Consider a swap between two replicas, i and j. After the swap, the new state of replica i will be the current

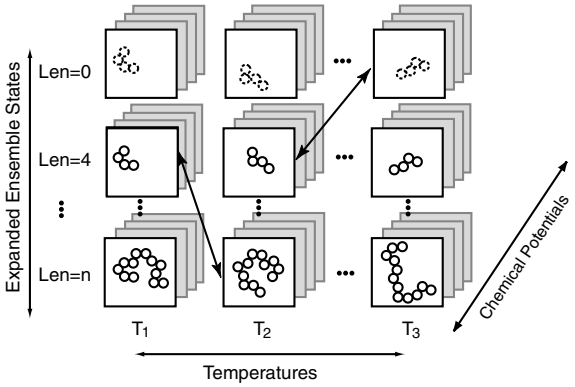

FIG. 1. Schematic illustration of the implementation of the hyperparallel Monte Carlo method. Each box represents a distinct replica of the simulated system; these replicas are simulated simultaneously in a single run. In addition to traditional Monte Carlo trial moves, these replicas can (1) change their state variables in the expanded dimension and (2) exchange configurations with each other, thereby visiting different values of T and μ.

state of replica j, and the new state of replica j will be the current one for replica i; i.e.,

$$\begin{aligned} x_i^{\text{new}} &= x_j^{\text{old}} \\ x_j^{\text{new}} &= x_i^{\text{old}}. \end{aligned} \tag{7}$$

Metropolis acceptance criteria are applied to trial swap moves. Given that simulations are being conducted in a composite ensemble of several replicas, a trial swap move is accepted with probability

$$p_{\text{acc}}(x_i \leftrightarrow x_j) = \min\left[1, \frac{w(x_j, \mathbf{f}_i) w(x_i, \mathbf{f}_j)}{w(x_i, \mathbf{f}_i) w(x_j, \mathbf{f}_j)}\right]. \tag{8}$$

The particular swapping acceptance criteria for hyperparallel tempering are obtained by substituting Eq. (6) into Eq. (8),

$$p_{\text{acc}} = \min[1, \exp(\Delta\beta \Delta U - \Delta N_y \Delta(\beta\mu))], \tag{9}$$

where $\Delta\beta = \beta_i - \beta_j$, $\Delta U = U_i - U_j$, $\Delta N_y = N_{y,i} - N_{y,j}$, and $\Delta(\beta\mu) = \beta_i \mu_i - \beta_j \mu_j$.

III. Applications

A. Lennard–Jones Fluid

The phase behavior of the Lennard–Jones fluid has been studied extensively in the past. It therefore provides an ideal example for examining the

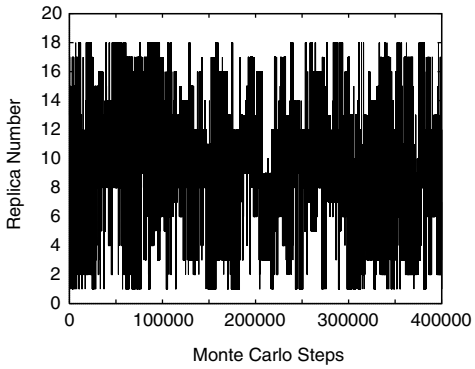

FIG. 2. Replica number as a function of Monte Carlo steps, for $T^* = 0.73$ and $\beta\mu = -5.30$.

performance and accuracy of HPTMC vis-à-vis those of other, more conventional methods. In this application, 18 replicas are simulated in parallel. Histogram reweighting techniques are employed to calculate the phase diagram of the system [22–24]. Figure 2 illustrates how replicas are swapped during a simulation. Each particular configuration or collection of particles can be labeled according to the replica number that it occupies at the beginning of a simulation. When a trial swap move is accepted, two configurations move to new replicas, and the transition is registered as a step change in the figure. Figure 2 describes the trajectory of configuration number 13 as it travels through different replicas during the course of a simulation. After a successful swap move, two replicas receive completely new configurations, thereby reducing dramatically the correlation time corresponding to a given thermodynamic state. Furthermore, through such swapping, configurations that were originally in low-temperature and high-density boxes can be passed over to high-temperature and moderate-density boxes, where they can relax more rapidly. Relaxed configurations can subsequently return to their original box, thereby accelerating the overall relaxation of the global system and facilitating sampling of phase space under adverse conditions. It is instructive to note that swapping provides an efficient way of sampling the tails of the distribution function corresponding to a given thermodynamic state; such tails often contribute significantly to thermodynamic averages, and they can be difficult to sample using conventional techniques.

Figure 3 compares the phase diagram calculated from histograms corresponding to all 18 replicas with literature data for the same fluid [26]. The two sets of data are in quantitative agreement [13]. The slight discrepancies at high temperatures are due mainly to different definitions of the equilibrium saturated density. (In this work, we regard the mean density corresponding to a peak of the distribution as the equilibrium value; Wilding *et al.* [26] define

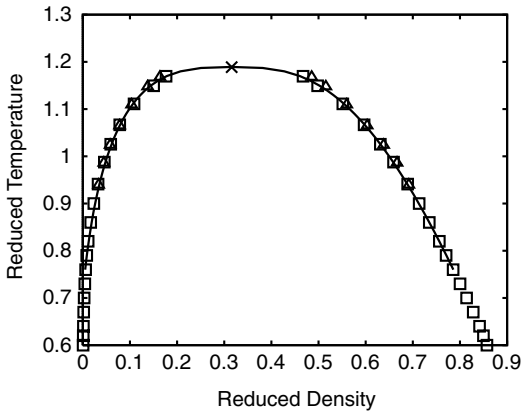

FIG. 3. Phase diagram (vapor–liquid equilibria) for a truncated Lennard–Jones fluid. The squares correspond with the results of this work, and the triangles show results reported by Wilding *et al*. [26]. Statistical errors are smaller than the symbol size. The solid line is an Ising form fit to the simulation data.

it as the peak value of the distribution.) As shown in Fig. 3, the proposed method is able to generate phase equilibrium data at temperatures and densities in the near vicinity of the triple point of the truncated Lennard–Jones fluid (e.g., $T^* = 0.60$ and $\rho^* = 0.86$). A simple Gibbs ensemble method or conventional grand canonical simulations would be much more demanding under such conditions.

B. PRIMITIVE MODEL ELECTROLYTE SOLUTIONS

Electrolyte solutions play a central role in chemical engineering practice. As such, they have been studied extensively (both theoretically and experimentally) in the past, but simulations have been limited. Simulations could provide much needed numerical data to verify the accuracy and validity of currently available, approximate predictions, and also yield useful insights for development of new theories. Primitive models provide one of the simplest representations of electrolyte solutions. In these models, the system is described by a binary mixture of charged hard spheres immersed in a dielectric continuum. Notwithstanding the apparent simplicity of the model, the calculation of the phase behavior of primitive electrolytes has presented a challenge to molecular simulations for several decades. The tendency of ions to associate, the long-range nature of Coulombic interactions, and the low temperatures that are often of interest in the study of electrolytes have all conspired to render such calculations particularly demanding. Primitive

model electrolytes are believed to exhibit a low-temperature gas–liquid region of coexistence [13, 27–31], and only recently has some consensus begun to emerge regarding the nature of the coexistence curve and the precise location of the critical point of the *restricted* primitive model (the special case in which both cations and anions have exactly the same size and charge) [31, 13]. The phase behavior of primitive models in general (having cations and anions of different size and charge) remains unknown, and researchers have had to rely on elaborate theoretical predictions to delineate the phase behavior of such systems [27, 32, 33].

We have used parallel tempering methods to study the general case of asymmetric primitive models. We use approximately 10 to 15 replicas in our calculations, and the composite system is simulated in parallel for at least 2×10^6 Monte Carlo steps to calculate a coexistence curve. Each Monte Carlo step consists of 200 particle displacements and 100 insertion or deletion attempts. Configuration swaps are attempted every 20 Monte Carlo steps. To estimate critical properties, four or five boxes are simulated in parallel for at least 10×10^6 Monte Carlo steps. Longer simulations are required as the asymmetry of the ions increases.

Figure 4 shows simulated binodal curves for asymmetric ionic systems. Coexistence curves are shown for $\lambda = 1, 0.75, 0.50$, and 0.25, where $\lambda = \sigma_+/\sigma_-$ is the ratio of the radius of cations and anions and therefore provides a measure of the asymmetry of the system. The results of our simulations indicate that as λ decreases from 1 (the restricted model) to 0.05 (the most asymmetric system considered in our simulations), both T_c^* and ρ_c^* decrease. For nearly symmetric electrolytes (e.g., $\lambda = 0.75$), the effect of λ is relatively

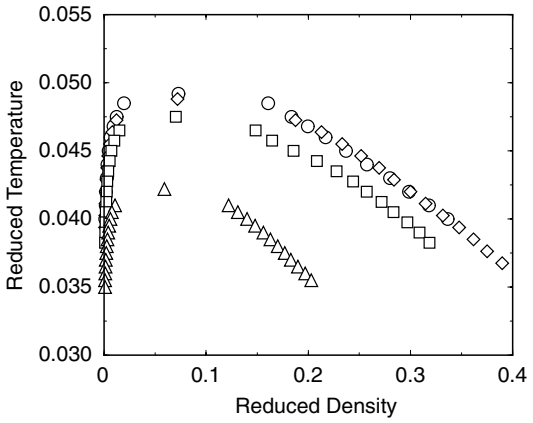

FIG. 4. Simulated binodal curves for size-asymmetric electrolyte systems with different λ values. Circles, $\lambda = 1$; diamonds, $\lambda = 0.75$; squares, $\lambda = 0.5$; triangles, $\lambda = 0.25$.

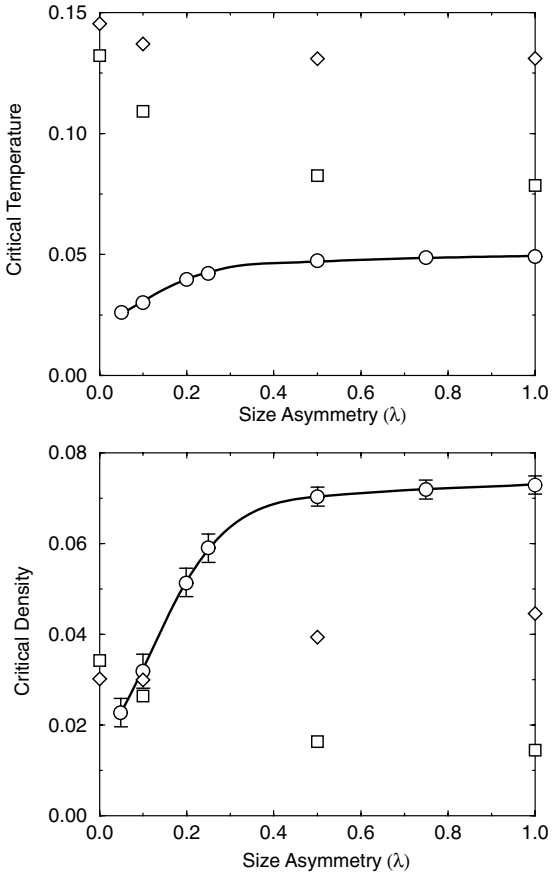

FIG. 5. Simulated binodal curves for size-asymmetric electrolyte systems with different λ values. Circles, $\lambda = 1$; diamonds, $\lambda = 0.75$; squares, $\lambda = 0.5$; triangles, $\lambda = 0.25$.

small. The binodal curves corresponding to $\lambda = 1$ and $\lambda = 0.75$ are almost identical. For highly asymmetric systems ($\lambda < 0.4$), the effect of λ is much stronger and the coexistence curves show pronounced differences.

The simulated behavior of T_c^* and ρ_c^* with size asymmetry can be compared to existing integral-equation theoretical predictions using a mean-spherical approximation (MSA). Figure 5 shows the simulated critical parameters as a function of the size asymmetry. Recently reported predictions of MSA are also shown for both the virial and the energy routes [27]. As expected from a mean-field calculation, the MSA critical predictions are not in quantitative agreement with the results of simulations. What is perhaps more surprising, however, is that the trends predicted by the theory disagree with

those observed in simulations. The MSA theory predicts that both the critical temperature and the critical density *increase* as λ decreases.

We have also examined the effects of charge asymmetry on the phase behavior of primitive electrolytes. For 2–1 electrolytes (the cation has a charge of 2, while the anions have unit charge), if the sizes of cations and anions are the same, the MSA theory predicts that the critical point is identical to that of the RPM (same anion–cation charge and size), namely, $T_c^* = 0.049$ and $\rho_c^* = 0.062$. Our simulations predict that the critical temperature is reduced significantly, to $T_c^* = 0.046$, and the critical density increases to $\rho_c^* = 0.105$.

A key feature of electrolyte systems is their tendency to associate. Figure 6 shows several clusters from a simulation of the $\lambda = 0.1$ system in a box of size $L^* = 55$ at $T^* = 0.03$. The instantaneous density is $\rho^* = 0.00122$. As shown in the figure, ions form polymer-like structures whose shapes include chains, rings, and branched chains. This pronounced tendency to cluster can be rationalized by considering a simple aggregate of only four ions. Figure 7 shows the fraction of ions involved in clusters of a given size n, for $\lambda = 0.1$, at $T^* = 0.03$ and $\langle \rho^* \rangle = 0.003$ (for comparison, we also show results for the RPM model at a similar density). The cluster size distribution exhibits an

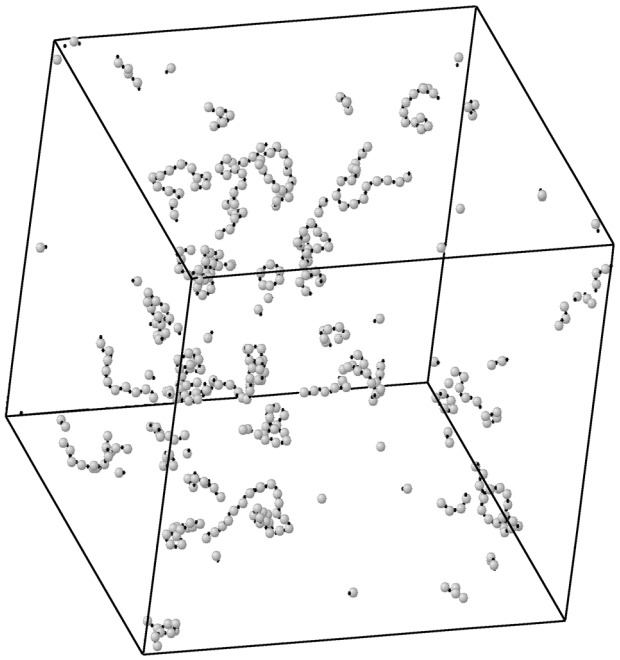

FIG. 6. Configuration representative of a size-asymmetric ionic system with $\lambda = 0.1$ and $L^* = 55$ at $T^* = 0.03$. The instantaneous density corresponding to this configuration is $\rho^* = 0.00122$.

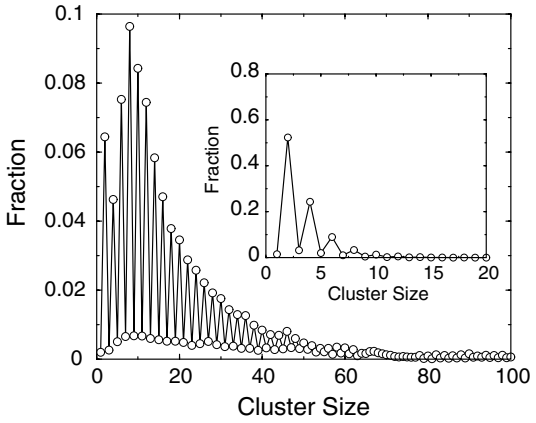

FIG. 7. Probability of finding an ion involved in a cluster of size n at $T^* = 0.03$ and $\rho^* = 0.003$ for a $\lambda = 0.1$ system of size $L^* = 91$. The inset shows results for symmetric electrolytes (RPM model) at $T^* = 0.051$ and $\rho^* = 0.002$ in a system of size $L^* = 50$.

interesting maximum at $n = 8$, indicating that at this density and temperature, ions are more likely to be part of an octamer than a dimer; furthermore, this distribution extends even beyond 100 ions. In contrast, for symmetric systems at approximately the same density, most of the ions associate into simple pairs and most of the clusters involve fewer than 10 ions. These results suggest that theories capable of describing the low-temperature phase behavior of electrolytes should take into consideration the many-body nature of clusters; theoretical efforts in that direction have appeared recently [32], and it will be interesting to compare predictions of those theories to the results of simulations.

C. Homopolymer Solutions and Blends

Polymeric fluids constitute another class of systems for which theory has made considerable progress in the last decades; simulations of the phase behavior and thermodynamic properties of polymers, however, have been scarce. Sampling the configuration space of polymeric molecules is computationally demanding, and advanced simulation methods are generally necessary to generate meaningful statistical averages for the properties of interest.

We begin by reviewing applications of the proposed HPTMC method to polymer solutions and blends. For pure polymer solutions, we simulate chains consisting of up to 16,000 sites for simple-cubic lattice models and 500 sites

for bond-fluctuation lattice models. For polymer blends, we simulate two highly asymmetric systems on a cubic lattice: in the first, polymers have 16 sites and 64 sites, respectively. In the second, polymer chains have 50 sites and 500 sites, respectively. Both blend systems are simulated at constant temperature and chemical potential. For all systems, each Monte Carlo step consists of 50% chain growth or shrinking moves and 50% local moves (kinkjump and crankshaft moves). Configuration swaps are attempted every 10 Monte Carlo steps. Depending on the conditions, 18 to 20 replicas are used to calculate phase diagrams.

To measure the performance of hyperparallel tempering, we perform a series of simulations using the *NVT* ensemble, the grand canonical ensemble, multidimensional parallel tempering in a grand canonical ensemble, an expanded grand canonical ensemble, and the HPTMC method; in all cases we examine the decay of the end-to-end vector autocorrelation function for the polymer, which provides a stringent test of efficiency for a polymer-simulation technique. Figure 8 shows some of our results. The dotted curve shows the decay of this function for the *NVT* ensemble; the relaxation is slow and reaches a value of approximately 0.6 after 5000 steps. The curve below that of the *NVT* ensemble corresponds to the grand canonical simulation; the decay is only marginally better than that for the *NVT* method. This is due to the extremely low molecule-insertion acceptance rate experienced in

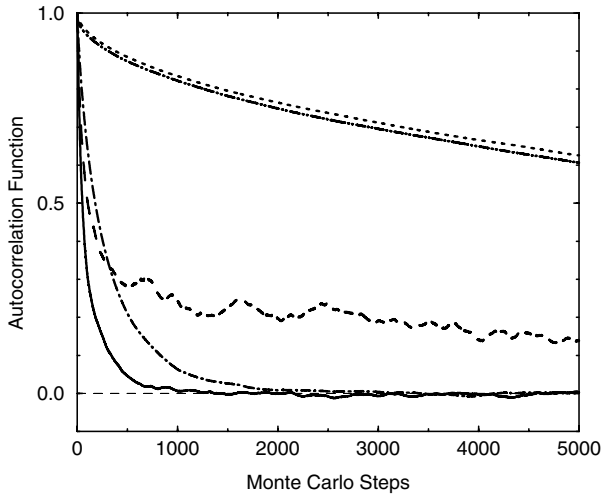

FIG. 8. End-to-end vector autocorrelation function for polymer chains obtained by different simulation methods: (1) short dashed line, canonical ensemble; (2) dash–dot–dotted line, grand canonical ensemble; (3) dashed line, multidimensional parallel tempering; (4) dash–dotted line, expanded grand canonical ensemble; (5) solid line, hyperparallel tempering.

conventional grand canonical simulations of macromolecules. The dashed line shows results from multidimensional parallel tempering simulations in the grand canonical ensemble; the performance is much better than that of naïve grand canonical or *NVT* simulations. The dash–dotted curve shows results for the *expanded* grand canonical ensemble; it decays to zero after about 3000 MC steps. The performance of the expanded grand canonical method is more than one order of magnitude better than that of a naïve grand canonical simulation. The solid curve shows the results for HPTMC; the decay to zero is even faster than for the expanded grand canonical method. The relaxation of the end-to-end autocorrelation function occurs in fewer than 1000 steps. In this context, HPTMC is several times more efficient than the expanded grand canonical technique, and more importantly, it is several orders of magnitude more efficient than some of the methods that have traditionally been used to simulate polymeric fluids.

Figure 9 shows coexistence curves for polymers of 100, 600, 1000, and 2000 sites. The lines are the results of this work, and the open symbols are simulation data from the literature [25]. For $n = 100$ and $n = 600$, our results are in good agreement with literature reports. Note, however, that with the new method, we are able to explore the phase behavior of long polymer chains down to fairly low temperatures. The computational demands of the new method are relatively modest. For example, calculation of the full phase diagram for polymer chains of length 2000 required less than 5 days on a workstation. It is important to emphasize that, for the cubic lattice model adopted here, chains of 2000 segments correspond to polystyrene solutions

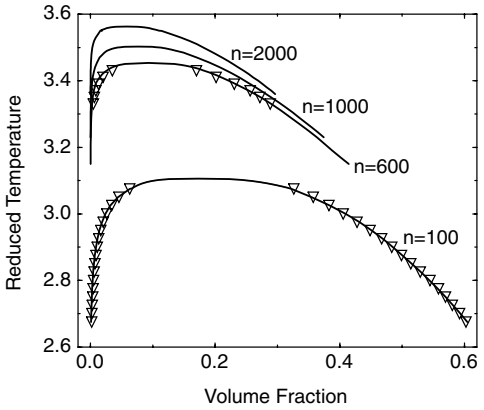

FIG. 9. Phase diagram for long polymer chains. The triangles are results reported by Panagiotopoulos and Wong [25]. The curves show results of this work. Note that with the HPTMC, we are able to calculate the phase diagram for longer polymers, down to lower temperatures, with modest computational requirements.

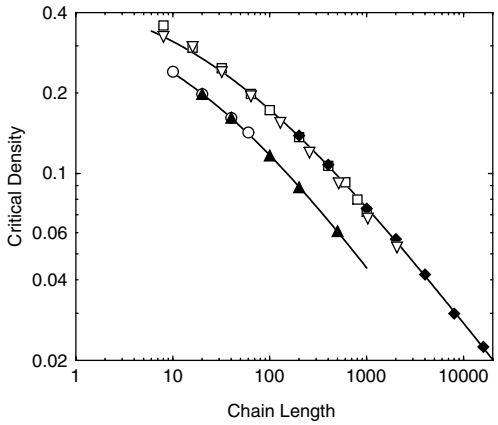

FIG. 10. Scaling of the critical density with chain length. The filled triangles show our results for the bond-fluctuation model, the circles are results reported by Wilding *et al*. [26], the diamonds show our results for the cubic lattice model, the open triangles are results reported by Frauenkron and Grassberger [38], and the squares are results reported by Panagiotopolous and Wong [25]. The curves are fits to our simulation results (using the functional form $\phi_c(n) = (b_1 + b_2 n^{x_2})^{-1}$). The uncertainty in the critical density is comparable to the size of the symbols.

of relatively high molecular weight (approximately 1,400,000). These are truly polymeric materials, and they therefore exhibit many of the key features (e.g., entanglement) that give rise to true polymeric behavior. The same calculation using traditional grand canonical or Gibbs ensemble techniques would require several months or years of computer time [34]. The results of simulations are also consistent with the experimental data for polystyrene–cyclohexane solutions [35, 36]. More importantly, our calculations indicate that, as shown in Fig. 10, for ultrahigh molecular weights, polymer solutions exhibit a crossover to classical scaling behavior [36]. This is contrary to the results of previous simulations for shorter polymers [25], but it is consistent with recent theoretical arguments by Grassberger and Frauenkron [38].

Another interesting application of HPTMC is encountered in the study of compressibility effects on the phase behavior of polymer blends. While much theoretical work has been devoted to describe the temperature dependence of miscibility for polymer blends, there are relatively few studies of the effect of pressure on miscibility. To a large extent, this is due to the fact that most theoretical models assume that polymer blends are incompressible. HPTMC can be used to determine the miscibility of blends as a function of pressure. Figure 11 shows the phase diagrams for two above-mentioned asymmetric polymer blends. For both of these systems, we can see that in

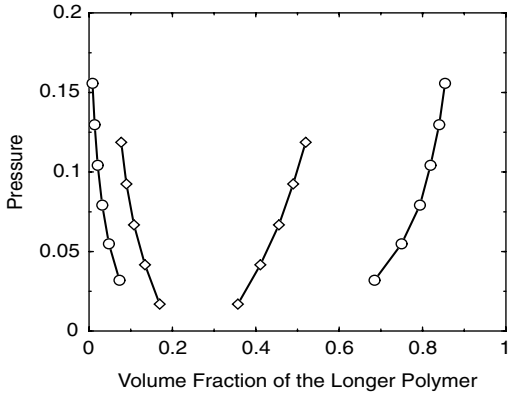

FIG. 11. Phase diagram for asymmetric polymer blends. Circles are for the system with chains of 16 and 64 sites ($kT/\varepsilon_{11} = 2.33, kT/\epsilon_{22} = 2.80, kT/\epsilon_{12} = 2.95$); diamonds are for the system with chains of 50 and 500 sites ($kT/\epsilon_{11} = 2.75, kT/\epsilon_{22} = 3.30, kT/\epsilon_{12} = 3.10$).

some circumstances the pressure can have a nonnegligible negative effect on the miscibility of the polymers. To the best of our knowledge, these results constitute the only available simulation report of the phase diagram of such highly asymmetric and compressible polymer blends; comparisons between our results and previous work are therefore not available at this time.

D. SEMIFLEXIBLE POLYMERS AND THEIR BLENDS WITH FLEXIBLE POLYMERS

We have also applied HPTMC to the simulation of phase coexistence for semiflexible polymers. As before, we use a lattice model to represent the polymers. Stiffness is modeled by introducing an energy penalty ε_B for each kink in a chain. For the particular system studied here, the chain length is $n = 100$, the energy penalty is $\varepsilon_B = 5$, the simulation box size is $L = 50$, and eight replicas are simulated in parallel.

Figure 12 shows the calculated vapor–liquid phase diagram of the semiflexible polymer system. The corresponding phase diagram for the fully flexible polymer is also shown in the figure. The stiffness of the polymer affects the phase diagram dramatically. The critical temperature is higher, and the critical density is slightly lower. The shape of the chains reveals several interesting features. As Fig. 13 shows, in the liquid phase chains adopt extended configurations to avoid energetic penalties; in the vapor phase, chains exhibit typical coiled configurations, similar to those encountered with flexible chains. At low temperatures, semiflexible chains also exhibit a transition to

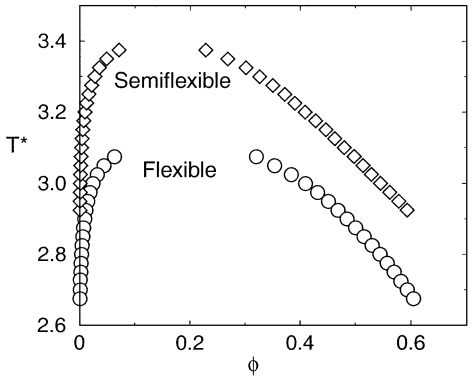

FIG. 12. Phase diagram for semiflexible polymer and fully flexible polymer. Circles are results for flexible polymers, and diamonds are results for semiflexible polymers. Both systems have a chain length $n = 100$. The bending energy penalty for the semiflexible polymer is $\varepsilon_B = 5$.

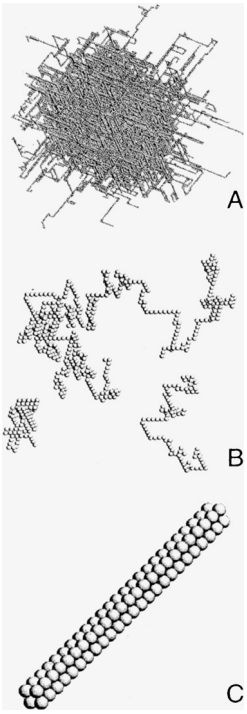

FIG. 13. Configuration snapshot of semiflexible polymer systems. (A) Saturated liquid phase at $T^* = 3.0$; (B) saturated vapor phase at $T^* = 3.0$; (C) single molecule at $T^* = 0.5$.

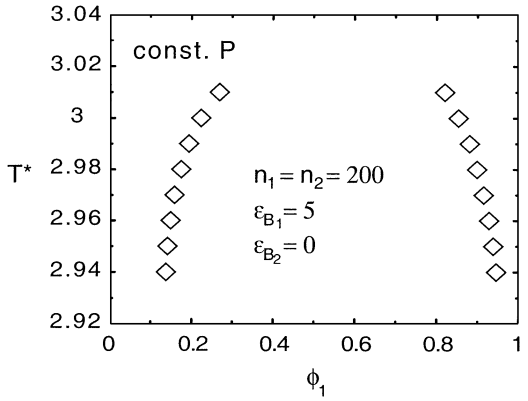

FIG. 14. Liquid–liquid phase diagram for a mixture of semiflexible and flexible polymers at constant pressure. The chain lengths of both species are $n = 200$.

more compact configurations. Figure 13 includes a configuration representative of some of the rod-like shapes that occur at $T^* = 0.5$.

Figure 14 shows the phase diagram of a flexible–semiflexible polymer blend at a constant pressure. Theoretical calculations and experimental results show that such mixtures can exhibit an isotropic–isotropic and isotropic–nematic phase separation. Our calculations are able to capture the isotropic–isotropic phase separation and serve to show that the origin of such a transition can be purely entropic.

E. Block Copolymers and Random Copolymers

As a last example of the application of HPTMC, we calculate the phase behavior of block copolymers and random copolymers. Again, lattice models are used in these calculations. For block copolymers, we study the influence of the number of blocks on the phase behavior; for random copolymers, we examine the effect of sequence length. We use a one-dimensional Ising model to represent the random copolymer. Sequence length is statistically determined by the "temperature" of the one-dimensional Ising model. When this "temperature" approaches infinity, the sequence of the copolymer is completely random; when the "temperature" approaches zero, the random copolymer becomes a diblock copolymer. For all calculations, the chain length is $n = 1000$.

Figure 15 shows the phase diagram of block copolymers and random copolymers. For comparison, the phase diagram of a homopolymer having the same molecular weight is also shown in the figure. As we can see, the number of blocks on the polymer has a dramatic effect on the phase behavior. The

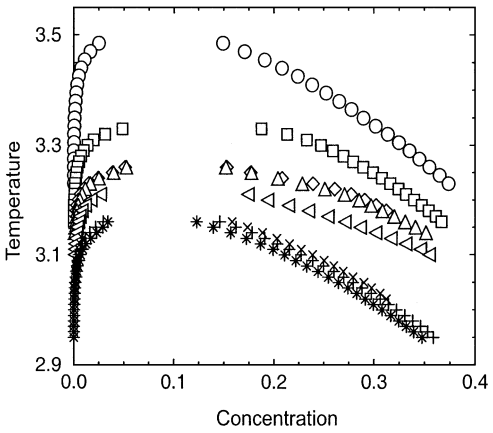

FIG. 15. Phase diagram of block copolymers and random copolymers. Circles are results for homopolymers; squares are results for diblock copolymers; diamonds are results for triblock copolymers; up triangles are results for a mixture of A–B–A and B–A–B triblock copolymers; left triangles are results for tetrablock copolymers; X's are results for random copolymers with average sequence length $l = 55$; crosses are results for random copolymers with $l = 20$; asterisks are results for a completely random copolymer.

coexistence curves for diblocks, triblocks, or tetrablocks lie well below that for the homopolymer; the critical temperature decreases as the number of blocks increases. In contrast, the coexistence curve for random copolymers is not affected considerably by the details of the "blocks" or their number. Our simulations indicate that the sequence length has only marginal effects on the phase behavior, at least as far as vapor–liquid coexistence is concerned.

IV. Discussion and Conclusion

Many of the applications described above, particularly the simulations of highly asymmetric electrolytes and long polymeric system, have been possible only through the use of the HPTMC method. The advantages of this new method have been shown to arise from the combination of biased, open ensemble simulations with replica swapping. Biased open ensemble simulations facilitate elimination of molecules from a simulation box and insertion into completely new positions and configurations; one needs not wait for particles to diffuse slowly through the system. Through replica swapping, the entire configuration residing in a simulation box can be completely replaced, thereby circumventing the slow diffusion through phase space that characterizes complex fluids.

Several factors affect the performance of HPTMC. First, factors that affect the performance of the underling expanded ensemble simulation clearly influence the performance of HPTMC. With regard to HPTMC itself, the frequency and success rate of configuration swaps are the most important factors. A simple rule-of-thumb that we have adopted in these applications is to make the frequency of successful swaps of the same order of magnitude as the frequency of successful particle insertions/removals. Note, however, that simulations of different complex fluids are likely to require some fine-tuning to arrive at optimal parallel tempering algorithms for complex fluids.

It is important to emphasize that, by construction, the acceptance rate for trial swap moves depends on the overlap between the probability distributions corresponding to the state points for two replicas; a high acceptance rate therefore requires closely spaced state points. This overlap depends on how far apart the state points of the replicas are, as well as the characteristics of the system. The width of the distribution functions decreases as the system size increases. For large systems, state points must be relatively close to achieve significant overlap. A possible solution to the problem is to combine further multicanonical sampling [1, 2] with HPTMC; by artificially widening the probability distribution, one should be able to simulate large systems and fewer boxes. Further studies in this direction are currently under way. A second shortcoming of the proposed method is the large memory required for simultaneous simulation of several boxes. This problem, however, can be alleviated by a parallel processor architecture.

In this paper, we have reviewed some recent applications of the HPTMC method. We have attempted to demonstrate its versatility and usefulness with examples for Lennard–Jones fluids, asymmetric electrolytes, homopolymer solutions and blends, block copolymer and random copolymer solutions, semiflexible polymer solutions, and mixtures. For these systems, the proposed method can be orders of magnitude more efficient than traditional grand canonical or Gibbs ensemble simulation techniques. More importantly, the new method is remarkably simple and can be incorporated into existing simulation codes with minor modifications. We expect it to find widespread use in the simulation of complex, many-molecule systems.

ACKNOWLEDGMENTS

This work was supported by the Division of Chemical Sciences, Office of Basic Energy Sciences, Office of Sciences, U.S. Department of Energy. Acknowledgment is also made to the Donors of the Petroleum Research Fund, administered by the ACS, for partial support of this research.

REFERENCES

1. Berg, B., and Neuhaus, T., *Phys. Lett. B* **267,** 249 (1991).
2. Berg, B., and Neuhaus, T., *Phys. Rev. Lett.* **68,** 9 (1992).
3. Hessebo, B., and Stinchcombe, R. B., *Phys. Rev. Lett.* **74,** 2151 (1995).
4. Lyubartsev, A. P., Martinovski, A. A., Shevkunov, S. V., and Vorontsov-Velyaminov, P. N., *J. Chem. Phys.* **96,** 1776 (1992).
5. Marinari, E., and Parisi, G., *Europhys. Lett.* **19,** 451 (1992).
6. Frantz, D. D., Freeman, D. L., and Doll, J. D., *J. Chem. Phys.* **93,** 2769 (1990).
7. Ortiz, W., Perlloni, A., and Lopez, G. E., *Chem. Phys. Lett.* **298,** 66 (1998).
8. Geyer, C. J., and Thompson, E. A., *J. Am. Stat. Assoc.* **90,** 909 (1995).
9. Marinari, E., Parisi, G., and Ruiz-Lorenzo, J., *in* "Directions in Condensed Matter Physics," (A. P. Young, Ed.), Vol. 12, pp. 59–98. Singapore, World Scientific (1998).
10. Tesi, M. C., Janse van Rensburg, E. J., Orlandini, E., and Whittington, S. G., *J. Stat. Phys.* **82,** 155 (1996).
11. Hansmann, U. H. E., *Chem. Phys. Lett.* **281,** 140 (1997).
12. Wu, M. G., and Deem, M. W., *Mol. Phys.* **97,** 559 (1999).
13. Yan, Q. L., and de Pablo, J. J., *J. Chem. Phys.* **111,** 9509 (1999).
14. Yan, Q. L., and de Pablo, J. J., *J. Chem. Phys.* **113,** 1276 (2000).
15. de Pablo, J. J., Yan, Q. L., and Escobedo, F. A., *Annu. Rev. Phys. Chem.* **50,** 377 (1999).
16. Wilding, N. B., and Binder, K., *Physica A* **231,** 439 (1996).
17. Escobedo, F. A., and de Pablo, J. J., *J. Chem. Phys.* **103,** 2703 (1995).
18. Escobedo, F. A., and de Pablo, J. J., *J. Chem. Phys.* **105,** 4391 (1996).
19. de Pablo, J. J., Laso, M., Siepmann, J. I., and Suter, U. W., *Mol. Phys.* **80,** 55 (1993).
20. Frenkel, D., Mooij, G. C. A. M., and Smit, B., *J. Phys. Condens. Matter* **4,** 3053 (1992).
21. Deleted at Proof.
22. Ferrenberg, A. M., and Swendsen, R. H., *Phys. Rev. Lett.* **23,** 2635 (1988).
23. Ferrenberg, A. M., and Swendsen, R. H., *Phys. Rev. Lett.* **63,** 1195 (1989).
24. Ferrenberg, A. M., and Swendsen, R. H., *Comput. Phys.* **Sept./Oct.** 101 (1989).
25. Panagiotopoulos, A. Z., and Wong, V., *Macromolecules* **31,** 912 (1998).
26. Wilding, N. B., Müller, M., and Binder, K., *J. Chem. Phys.* **105,** 802 (1996).
27. González-Tovar, E., *Mol. Phys.* **97,** 1203 (1999).
28. Panagiotopoulos, A. Z., *Fluid Phase Equil.* **76,** 97 (1992).
29. Caillol, J. M., *J. Chem. Phys.* **100,** 2161 (1994).
30. Orkoulas, G., and Panagiotopoulos, A. Z., *J. Chem. Phys.* **101,** 1452 (1994).
31. Orkoulas, G., and Panagiotopoulos, A. Z., *J. Chem. Phys.* **110,** 1581 (1999).
32. Bernard, O., and Blum, L., *J. Chem. Phys.* **112,** 7227 (2000).
33. Raineri, F. O., Routh, J. P., and Stell, G., *J. Phys. IV* **10,** 99 (2000).
34. Panagiotopoulos, A. Z., *Mol. Phys.* **61,** 813 (1987).
35. Dobashi, T., Nakata, M., and Kaneko, M., *J. Chem. Phys.* **72,** 6685 (1980).
36. Yan, Q. L., and de Pablo, J. J., Critical behavior of lattice polymers studied by Monte Carlo simulations, *J. Chem. Phys.* **113,** 5954 (2000).
37. Deleted at Proof.
38. Frauenkron, H., and Grassberger, P., *J. Chem. Phys.* **107,** 9599 (1997).
39. Dudowicz, J., and Freed, K. F., *Macromolecules* **24,** 5074 (1991).
40. Gromov, D. G., and de Pablo, J. J., *J. Chem. Phys.* **109,** 10042 (1998).